BAR-ILAN UNIVERSITY

Efficient Interaction of Heralded X-ray Photons with

a Beam Splitter

Edward Strizhevsky

Submitted in partial fulfillment of the requirements for the Master's Degree

in the Department of Physics, Bar-Ilan University

Ramat-Gan, Israel   **2021**

This work was carried out under the supervision of

Prof. Sharon Shwartz

Department of Physics, Bar-Ilan University

Acknowledgments

Table of Contents

Abstract

In this work I present the first experimental demonstration of efficient interaction of multi-kilo-electron–volt heralded single x-ray photons with a beam splitter. This beam splitter and the experimental setup were used to show the sub-Poissonian statistics of a single photon state of radiation. I was the first author in a paper that describes these results and which was published in Physical Review Letters [1]. In addition, I presented these results in an oral talk at CLEO conference [2].

Beam splitters are fundamental components in quantum optics that are used to demonstrate superposition of photon states and light intensity correlations and are routinely used in a broad range of wavelengths [3]. However, even for the most promising sources of single x-ray photon, the existing beam splitting devices are very inefficient, due to the broad spectral and angular spread of the generated single photons. In my work I utilized an efficient beam splitter with a mosaic crystal. A 'mosaic' crystal is a name of a model for crystal imperfections. According to this model, a real crystal is made of a mosaic of small misoriented crystal blocks [4]. For estimation of the efficiency and for the comparison with the theory I modeled it by an analytical function and estimated numerically the required parameters for efficient interaction with our single x-ray photon source. The source is a nonlinear crystal that I used for the generation of pairs of photons by using the effect of spontaneous parametric down conversion. The model predicts that the ratios between the rates of the reflected and transmitted heralded photons and the rate of heralded photons in the absence of the beam splitter are $r_{\text{R-Model}}=0.13$ and $r_{\text{T-Model}}=0.17$, respectively. I measured and compared the count rate of the incident broadband heralded photons in the absence of the beam splitter and after its introduction to find its efficiency. I found that the measured heralded photon rate at the outputs of the beam splitter is about 0.01 counts/s which is comparable to the measured rate in the absence of the beam splitter - 0.0583 ± 0.0099 counts/s. The count rates that I measured after the beam splitter show that it is efficient enough to measure single photon statistics.

After I showed that the mosaic crystal beam splitter is efficient, I used it to demonstrate the quantum statistics of heralded photons. I verified that the beam splitter preserves the sub-Poissonian statistics by showing that the degree of correlation at both its outputs is zero. Finally, I performed the fundamental demonstration of quantum optics - single photon interaction with a beam splitter. I obtained the well-known result that a photon

cannot split by measuring 2264 heralded single photons while all of them were either transmitted or reflected by the beam splitter but never both.

My experiment demonstrates the major advantage of x-rays for quantum optics – the possibility to observe experimental results with high fidelity and with negligible background. The practically noiseless measurements were possible due to the high energy of the x-ray photons and the commercially available silicon drift detectors (SDD) that not only have a very low dark current but are also photon number and energy resolving. While I did not show yet fields interference but intensity correlations, a major challenge for performing quantum optics experiments with x-rays was an efficient beam splitter and my work shows its implementation.

1. Introduction

The extension of quantum optics to x-ray energies would have a tremendous impact, but till now it was limited by the absence of efficient optical components [5]. The x-ray regime could introduce nearly perfect detectors while quantum optics would make it possible to reduce the x-ray ionizing radiation doses. However, despite the pronounced potential, the utilization of optical components has never been demonstrated with x-ray **quantum light** sources. My work focuses on beam splitters, which are essential components for quantum optics. The main challenge is finding beam splitters that can facilitate the broad spectral and angular widths of the generated quantum states of x-ray radiation.

The combination of x-ray regime with quantum optics is beneficial for both fields. Quantum optics could take advantages of the commercially available x-ray detectors that reach nearly 100% efficiency with low dark current and real photon number resolving capabilities over a very broad spectral range. Moreover, in the last decade, 2D x-ray detectors with similar performances are becoming available [6,7]. The benefits for the x-ray regime from concepts of quantum optics are a significant reduction of radiation doses used for imaging [8–10], an enhancement of the sensitivity [11], and the improvement of the signal-to-noise ratio (SNR) of measurements [12–17] – which are all very important since x-ray energies are ionizing radiation, hence there is a possibility of radiation-induced damage. Photons in x-ray spectral region have sufficient energy to break chemical bonds and ionize atoms, which can cause chemical and structural damage, potentially affecting critical function [18].

The above mentioned advantages of x-ray regime are extremely appealing for tests of basic concepts in quantum optics [5,19] however, beam splitters are required. Beam splitters, which are devices that split electromagnetic radiation, are among the most important optical components for quantum optics [20–23]. They are the essential components in almost any experiment aiming at the study of fundamental quantum optics and serve as the building blocks for almost any optical quantum technology. Indeed, seminal works showing the quantum nature of light using beam splitters include, for example, the Hong-Ou-Mandel effect [24], interaction free measurements [25,26], interaction of single photons with a beam splitter [27], and the generation and measurements of entanglement [28] and NOON states [29]. The first step towards

1

exploiting x-ray benefits for these fundamental demonstrations of quantum optics is finding an efficient beam splitter.

Existing beam splitting devices are inefficient with well-established x-ray quantum light sources but there are a few possible solutions. The two potential sources for the generation of nonclassical forms of radiation in the x-ray regime are radioactive sources with a cascade scheme that leads to the emission of two simultaneous photons and spontaneous parametric down-conversion (SPDC) in which pairs of entangled photons are generated [30]. The first has been demonstrated with Mossbauer nuclei [31,32] but although exhibits a very narrow spectral range, the emission is in all directions, thus it is challenging to collect a sufficient portion of the emerging photons. In SPDC the spectral width of the generated photons is in the multi-keV range and the angular width is several degrees [33–35]. However, in most cases, x-ray optics relies on either Bragg scattering or on reflection from surfaces [4]. For Bragg scattering from crystals the typical values for the angular acceptance and spectral width are a few mdeg and eV, respectively. Accordingly, those devices cannot render the interaction with the broad SPDC signal efficiently. Reflections from surfaces work well only at grazing incident angles and cannot be used either. The two conceivable candidates are mosaic crystals [4,36] and nanoscale multilayer periodic structures [18]. Both can be designed to support acceptance angles in the several degrees range and with spectral line shapes exceeding several hundred electron-Volts. However, the parameters have to be selected carefully to maintain high simultaneous reflectance and transmittance.

In this work I describe how to utilize broad spectral and angular bandwidth x-ray beam splitters for x-ray quantum optics. I use the broadband heralded photons generated by SPDC as a quantum state and show that their interaction with the beam splitter is efficient by comparing the coincidence rates before and after the beam splitter. My approach to realize efficient interaction is to use a mosaic crystal as a Bragg beam splitter with a wide rocking curve width and to choose its angular dispersion to match the angular dispersion of the photon pairs. I prefer the mosaic crystal over multilayers to avoid the loss in the substrate of those devices. I employ the beam splitter to demonstrate directly and without background noise that for a single x-ray photon there is nominally perfect anticorrelation between the events at the output ports of the beam splitter despite the unavoidable loss in the system. This is in agreement with the prediction of Barnett et al. who considered a quantum theory for the interaction with lossy beam splitters [37].

2

2. Background

2.1. X-ray single photons - generation and nonclassical behavior

The isolation of a single-photon light state is achieved by heralding one photon from a photon pair. The source of these photon pairs is the SPDC process. In SPDC a pump photon of frequency ω_p is destructed, and two photons (initially in their vacuum states) are created simultaneously by a spontaneous emission in a nonlinear crystal [3]. The two generated photons are coupled by the nonlinear coefficients and this coupling is used to calculate the rate of pairs that are leaving the crystal [33]. The photon pair conserve energy with the pump photon and their momentum conservation with the crystal (which is also called phase matching) dictates the angles of propagation [38]. Since the photons are always generated in pairs, once we detect one photon (which I call Trigger), we know with certainty that the second photon exists. This second photon, that I call Heralded, exhibits all the properties of single photons including sub-Poisson statistics, which is a clear distinction from classical radiation.

Of interest to the present work is that a true single photon cannot split even when it interacts with a beam splitter in contrast to classical beams. I use the term 'split' to describe the division of the input electromagnetic energy. A single photon can be either transmitted or reflected by a beam splitter thus detected at either of its output ports but not at both simultaneously [3,22,27,39–42]. This type of experiment is called Brown-Twiss interferometer [43] and expressed in terms of the quantum degree of second-order coherence $g^{(2)}$. The function $g^{(2)}$ is the normalized intensity correlation between the two outputs of the beam splitter. For example, in the case of a single mode electromagnetic field at one of the beam splitter input ports, the normalized correlation is $g_{3,4}^{(2)} = \frac{\langle n_3 n_4 \rangle}{\langle n_3 \rangle \langle n_4 \rangle} = \frac{\langle n_1(n_1-1) \rangle}{\langle n_1 \rangle^2}$, where n_3, n_4 are the photon numbers at the outputs of the beam splitter and n_1 is the photon number at the input to the beam splitter. For a single photon interaction with the beam splitter ($n_1 = 1$), the correlation is zero, which means that there will never be a simultaneous measurement at the two outputs. This result of zero correlation could be also shown for the more general case of a single photon wave-packet at the beam splitter input [3]. This behavior, which has no classical analog, is manifested in the coincidence measurements between the two output ports of the beam splitter, which are null when using ideal single photon sources

and detectors. I note however that beam splitters divide the field operators of single photons as observed with single photon interferometers [3,27].

2.2. Calculation of the heralded photon rate

To find parameters that can support high-efficient beam splitter interaction with single photons I calculate numerically the rate of the heralded photons by using the second order Glauber correlation function [33] where I consider a Gaussian function to model the reflection coefficient of the beam splitter.

Since the count rates of heralded photons are actually the coincidence count rates between the heralded photons and the trigger photons, I need to calculate the coincidence count rate between each of the output ports of the beam splitter and the trigger detector. I use the second order Glauber correlation function, which is given by

$R_c = S \iint \left\langle a_{Trig}^\dagger \left(\mathbf{r}_2, t_2 \right) a_{Heral}^\dagger \left(\mathbf{r}_1, t_1 \right) a_{Heral} \left(\mathbf{r}_1, t_1 \right) a_{Trig} \left(\mathbf{r}_2, t_2 \right) \right\rangle d\mathbf{u} d\tau$ where S is the area of

the pump at the input of the nonlinear crystal, $\mathbf{u} = \mathbf{r}_2 - \mathbf{r}_1$, and $\tau = t_2 - t_1$ [33]. Since it is more convenient to calculate the frequency domain operators than the time-space

operators I use the relation $a_j \left(z, \mathbf{r}, t \right) = \int_0^\infty \int_{-\infty}^\infty a_j \left(z, \mathbf{q}, \omega \right) \exp \left[-i \left(\mathbf{q} \cdot \mathbf{r} - \omega t \right) \right] d\mathbf{q} d\omega$,

where $\mathbf{r} = (x, y)$ and $\mathbf{q} = (k_x, k_y)$ to transfrom the operator to the frequncy domain (in time and in space). The relation between ω, the photon angular frequency, and the magnitude of the wave-vector is $\omega_j = k_j c / n \left(\omega_j \right)$ and the wave-vector components k_x and k_y are parallel to the surfaces of the nonlinear crystal. The operators satisfy the commutation relations -

$[a_j \left(z_1, \mathbf{q}_1, \omega_1 \right), a^\dagger_k \left(z_2, \mathbf{q}_2, \omega_2 \right)] = \dfrac{1}{\left(2\pi \right)^3} \delta_{j,k} \delta \left(z_1 - z_2 \right) \delta \left(\mathbf{q}_1 - \mathbf{q}_2 \right) \delta \left(\omega_1 - \omega_2 \right).$

To calculate the frequency domain Heralded and Trigger operators, first, their values at the output of the nonlinear crystal are calculated by solving the lossless coupled equations assuming the undepleted pump approximation in the Heisenberg picture

$$\frac{\partial a_{Heral}}{\partial z} = \kappa a_{Trig}^\dagger \exp \left(i \Delta k_z z \right)$$

$$\frac{\partial a_{Trig}^\dagger}{\partial z} = \kappa^* a_{Heral} \exp \left(-i \Delta k_z z \right)$$

(1)

Here κ is the coupling constant that includes the nonlinear coefficient and the pump intensity and $\Delta k_z = k_p \cos(\theta_p) - k_{Heral} \cos(\theta_{Heral}) - k_{Trig} \cos(\theta_{Trig})$ is the phase mismatch along the z direction. θ_p, θ_{Heral}, and θ_{Trig} are the angles between the atomic planes and the wave vectors of the pump, heralded, and trigger photons, respectively.

3. Numerical Model and Experimental Setup

3.1. Efficiency of the beam splitter with heralded photons

For the efficiency calculation I need to incorporate the expression that presents the beam splitter. The aim of this numerical simulation is to examine how the parameters of the mosaic crystal impact its efficiency as a beam splitter for the down converted photons, which possess broad energy and angular distributions. However, there is no simple analytical expression for the reflection coefficient for mosaic crystals [4], and I wanted the model to be as clear as possible, so that the important parameters could be easily identified and characterized. Therefore, I used a Gaussian model for the reflection coefficient and neglected the additive quantum noise from the open port of the beam splitter. The latter is justified since, for the efficiency calculation, I am interested in the mean output photon numbers of the heralded photons (the correlation between the trigger and one of the output ports of the beam splitter) and not trying to calculate the correlation between the output ports of the beam splitter [3]. The Gaussian function that I chose for the model was -

$$R\left(\omega_{Heral}, \Delta\theta\right) = \sqrt{A} \exp\left\{-\frac{1}{2}\left[\frac{\Delta\theta + \theta_B\left(\frac{1}{2}\omega_p\right) - \theta_B\left(\omega_{Heral}\right)}{b}\right]^2\right\}$$

(2)

This model incorporates the important parameters and describes reasonably the dependence of the reflectance of the mosaic crystal on the deviation from the Bragg angle and its spectral dependence. Here the frequency dependence is originated from the Bragg's law for a given incident beam frequency $\theta_B\left(\omega_{Heral}\right) = \sin^{-1}\left(\frac{\pi c}{d\omega_{Heral}}\right)$,

where c is the speed of light and d is the lattice interplanar spacing. The angular deviation $\Delta\theta$ is defined relative to the Bragg angle at the heralded photon wavelength as described in Fig. 1. The peak reflectivity is denoted by A and b is the width parameter which is deduced from the Full Width at Half Maximum (FWHM) of the rocking curve of the mosaic crystal.

In this work I chose to use a Highly Ordered Pyrolytic Graphite (HOPG) for the beam splitter. The HOPG is a good candidate for a beam splitter due to its availability, high reflectivity and low absorption [36,44,45]. The numerical calculations for its

performance are shown in chapter 4.1. The peak reflectivity A of HOPG is taken to be 0.5 [36]. The width parameter b is $0.48°$ and it was calculated form the measured rocking curve FWHM of the HOPG at our laboratory, which is $0.8°$.
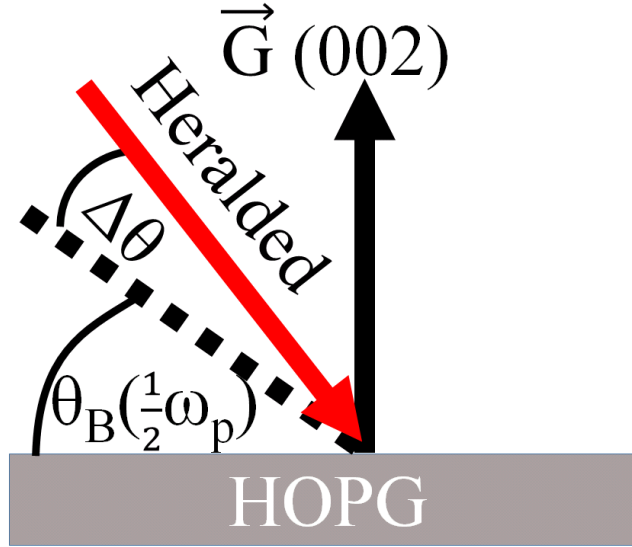

FIG. 1. Description of the angles of the beam that hits the beam splitter.

Finally, I multiplied the heralded operator I found by solving Eq. 1 by the expression in Eq. 2 and calculated the coincidence count rate by numerically integrating over photon energies in the range of 9.5 keV to 11.5 keV and an angular range of 5 mrad centered at the phase matching angle, which covers an area of about 20 mm^2 on the detector (further details are described in chapter 3.2).

I show below that the important parameter is the Bragg angle that for a given input wavelength is determined by the lattice interplanar spacing, thus can serve as a guide for the selection of the material and the crystallographic orientation of the beam splitter. In Fig. 2 I show the theoretical dependence of the heralded photon count rate on the Bragg angle of the beam splitter for my experimental parameters (which are described in chapter 3.2). From Fig. 2 I concluded that we need to choose the smallest possible Bragg angle to enable the largest energy bandwidth as can be estimated also by calculating the differential of Bragg's law. This conclusion is general and independent of the details of the experiment. In addition, for a fixed lattice spacing, there is a linear dependence between the rocking curve width of Bragg scattering of the beam splitter and the count rate of the heralded photons. For example, for the parameters described above, increasing the rocking curve width by a factor of a hundred leads to an enhancement of the count rate by about 90.

Of importance, although the mosaic spread deteriorates the reflectivity, it should be sufficiently broad to accommodate the broad angular and spectral distributions of the SPDC process. This tradeoff is important for the design of further x-ray quantum optics experiments with mosaic crystals. Another consideration is the loss in the transmitted beam, which increases when the incident angle of the photons impinging upon the beam splitter decreases. Using a thinner crystal could reduce the absorption but at the expense of the reduction of the reflectivity [36]. Finally, I also note that x-ray fluorescence should be considered when choosing the material for the beam splitter. Its characteristic energy must be sufficiently separated from the heralded photon energy.
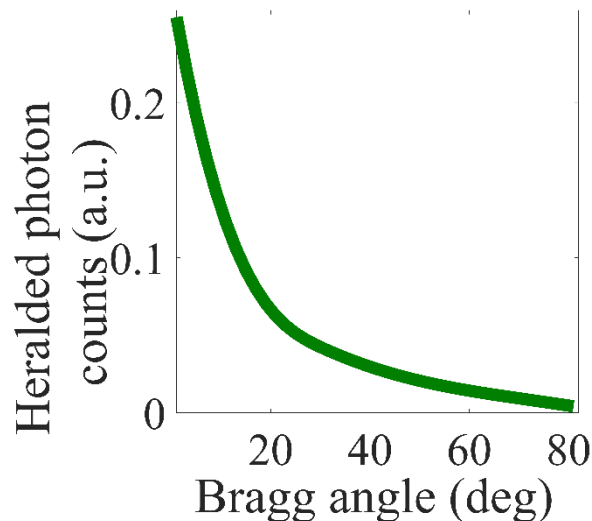

FIG. 2 Simulation results: normalized counts of the heralded photons that are Bragg scattered by the beam splitter as a function of the Bragg angle of the beam splitter. The vertical axis is normalized by the coincidence counts at the output of the SPDC crystal and is corrected for absorption in air assuming a 10 cm of air path between the SPDC crystal and the detectors.

3.2. Experimental setup

The setup I used in this work and that is based on the standard scheme for generating and detecting heralded photons [33] is depicted in Fig. 3. In this scheme a pump beam at $\hbar\omega_p = 21$ keV hits upon a nonlinear crystal, which is a diamond crystal, to generate photon pairs both at a central photon energy of 10.5 keV by SPDC. The reciprocal lattice vector normal to the C(660) atomic planes was used for phase matching, and the detectors were silicon drift detectors (SDDs) [38]. The dimensions of the diamond crystal were 4 mm × 4 mm × 0.8 mm. The theoretical value of the Bragg angle of the

C(660) atomic planes is 44.61°. For the beam splitter I used HOPG with the dimensions of 20 mm × 20 mm × 0.7 mm. I used its (002) atomic planes where the Bragg angle is 10.1° for the central photon energy (10.5 keV). The SDDs have an active detection area of 25 mm^2. For each photon pair, one photon at $\hbar\omega_{\text{Trig}}$ is denoted as the trigger photon and was measured directly by the detector D$_{\text{Trig}}$. The second photon at $\hbar\omega_{\text{Heral}}$ is the heralded photon and hits upon a beam splitter. It was collected by either D$_{\text{Ref}}$ or D$_{\text{Trans}}$, which were the detectors for the reflected and transmitted beams, respectively. For the generation of the photon pairs, I rotated the angle of the diamond crystal by 0.008° from the Bragg angle and set the angles of the trigger detector and the beam splitter with respect to the diamond atomic planes to 43.63° and 45.59°, respectively, according to the phase matching condition.

The experiment was performed at beamline P09 [46] of the PETRA III synchrotron storage ring (DESY, Hamburg). The distance between the detectors and the diamond crystal was 1000 ± 10 mm where a helium tube of 900 ± 10 mm length and 200 ± 5 mm diameter was used to reduce air absorption and scattering. The synchrotron beam dimensions were about 2 mm and 0.2 mm in the vertical and horizontal directions, respectively.

To separate the photon pairs from the background we used logic gates to register only coincidental detection events in which D$_{\text{Trig}}$ clicks together with either D$_{\text{Trans}}$ or D$_{\text{Ref}}$. The time window of the coincidence recording was about 800 ns (except for the results in Fig. 7). To distinguish the down-converted pairs from accidental coincidence counts I post-selected photons according to their energies using the photon energy resolving capability of our detectors. I recorded only photons with photon energies in the range from 7 keV to 17 keV and that the sum of their photon energies was within an energy window of 1 keV around the energy of the pump photon in accord with the conservation of energy and the resolution of our system. I collected also data with wider energy ranges, which is presented in Fig. 7 and Fig. 8. I used various energy ranges in order to compare the heralded photons with the classical beam.
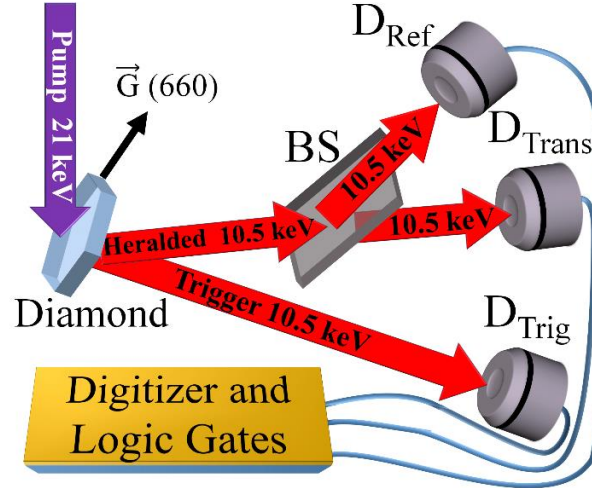
FIG. 3. Experimental setup. The photon pairs are generated in the diamond crystal. The trigger photons are collected by detector D_{Trig} and heralded photons hit the HOPG crystal that is utilized as a beam splitter (BS). D_{Trans} and D_{Ref} are the detectors for the transmitted and reflected (Bragg scattered) photons, respectively.

3.3. Coincidence electronics and data acquisition

Here I provide further details on the coincidence electronics, which was used to verify that the photon pairs arrive simultaneously and to reduce background radiation. The detectors generate two types of signals for each detected photon: analog voltage pulses with height that is proportional to the photon energy of the detected photons and logic pulses with a fixed height of 1.4 V. The pulse duration of the analog signal is 200 ns and the pulse duration of the logic signal is 1000 ns. The logic pulse is generated only when a photon within a predefined energy range is detected (functions as an output of a single channel analyzer).
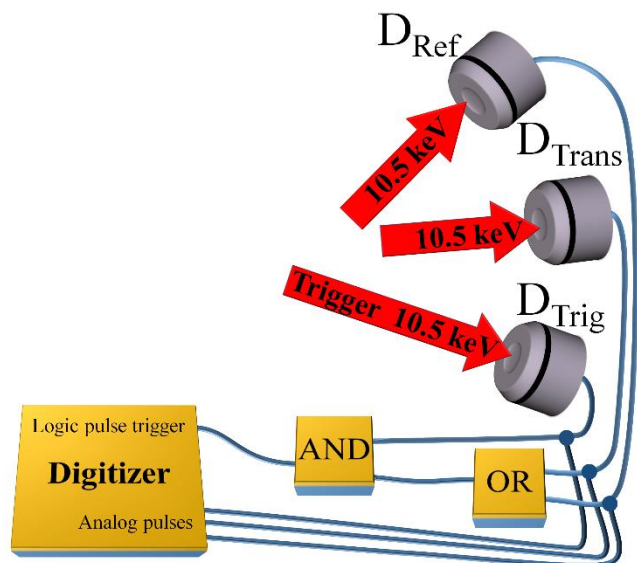
FIG. 4. Schematic of the coincidence electronics.

As can be seen in Fig. 4 I used logic gates to trigger a digitizer when the logic pulses from detector D_{Trig} and at least one of the detectors D_{Trans} or D_{Ref} overlapped. The overlap point is determined by the beginning of overlap between two logic pulses. I used logic gates triggering since otherwise the raw count rate of the detector would lead to overflow of the buffer of our digitizer. These logic gates reduced the number of the event rates that were registered by the digitizer to less than 200 events per second. After the measurement I scanned the data and used a software filter to register only events that their analog pulses were within a time window of ± 800 ns around the overlap point. This procedure improved the signal-to-noise ratio as can be seen from the background free results presented in chapter 4.3. However, if two photons were separated by 800-1000 ns they still could trigger the digitizer (due to the length of the logic pulses), but one of them is partially outside the time window of the software filter, which restricts the detection window to 1600 ns, as shown in Fig. 5. In this case only the photon in the window that was allowed by the software is registered, thus the system registers an event with only one photon and not a pair of photons. I can of course use the software to filter out events that are not the detection of pairs of photons, but I used it to demonstrate the reduction in σ as it is shown in Fig. 7 of chapter 4.2.
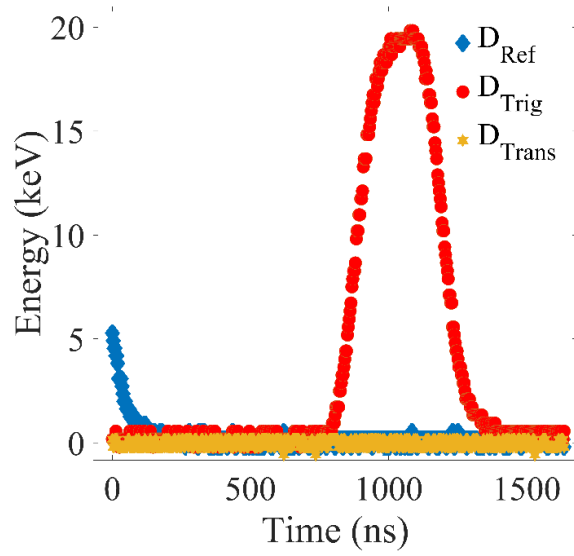
FIG. 5. An example for measured digitizer traces when only detector D_{Trig} was recorded. In this example detector D_{Trig} detected a photon at about 20 keV. Detector D_{Ref} also detected a photon in the photon energy window allowed by our system and the digitizer was triggered to record the analog signal. However, the temporal separation between the two analog signals was larger than 800 ns, and the analog signal of detector D_{Ref} was not registered.

4. Results

4.1. The efficiency of the beam splitter

I first show that the interaction between the heralded photons and the beam splitter is efficient by exploring the count rates of the heralded photons at each of the output ports of the beam splitter. Figures 6(a) and 6(b) show the spectra of the measured heralded photon counts for the reflected and the transmitted photons, respectively. For the comparison I show the measured spectrum of the trigger detector and plot the numerical calculations for the two spectra. The total heralded photon count rates of the reflected and transmitted photons are n_R=0.0093±0.0003 photons/s and n_T=0.0164±0.0004 photons/s respectively and were measured for 88010 seconds. These rates are only slightly smaller than the heralded photon count rate that were measured before I inserted the beam splitter, n_H=0.0583±0.0099 photons/s, and are comparable to the measured coincidence rates in the previous experiments with similar input beam parameters where the photon pairs were measured directly after the nonlinear crystal [33,35,38]. **The total beam splitter efficiency is about 50% and this is a clear indication that the interaction of the heralded photons with the beam splitter is efficient.** For these experimental parameters the model (that is described in chapter 3.1) predicts that the ratios between the rates of the reflected and transmitted photons and the rate of the photon pairs in the absence of the beam splitter are $r_{R\text{-Model}}$=0.13 and $r_{T\text{-Model}}$=0.17, respectively. These values also quantify the inefficiency of the beam splitter, which originates from the differences between the acceptance angle of the mosaic crystal and the angular spread of the SPDC effect as well as the absorption. An additional effect that was not taken into account is Compton scattering since it is orders of magnitude weaker than reflection. The ratios I measured - r_R=0.159±0.027 and r_T=0.281±0.048 - are slightly higher, suggesting that the interaction with the beam splitter is more efficient than predicted. However, this discrepancy can be explained by the improvement in the alignment of the detectors between the two measurements and by a nonlinear response of the detectors due to the strong background in the absence of the beam splitter.

Figure 6 also indicates that, as expected, the measured spectrum of the reflected photons is narrower than spectrum of the transmitted photons since they are Bragg reflected and the agreement between the experimental results and the theory is within the experimental uncertainties. The theoretical dip in the curve of the transmitted beam

(Fig. 6(b)) is attributed to Bragg scattering at the energy corresponding to the Bragg angle and cannot be seen in the measurements due to the insufficient energy resolution of the setup. Moreover, the calculated reduction of the transmitted beam counts (Fig. 6(b)) at lower energies arises from the larger x-ray absorption. The histogram binning and the energy resolution of the detection system smear the sharp decrease in absorption at the higher end of the spectrum.
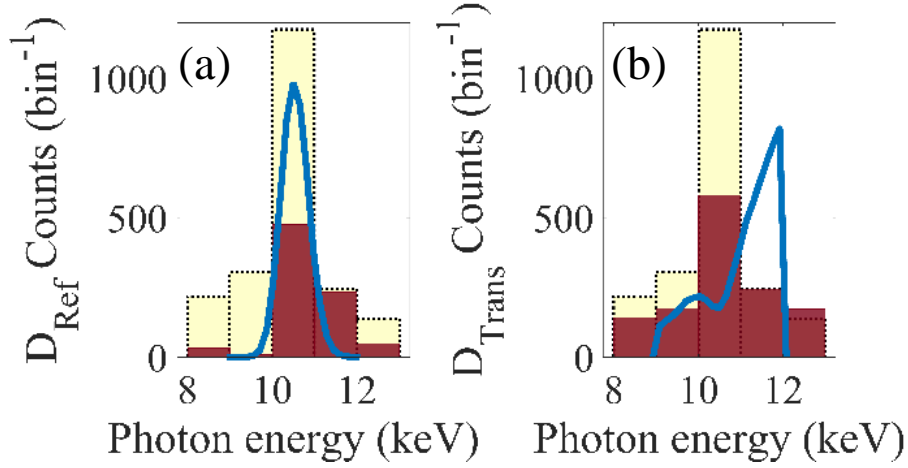

FIG. 6. Photon energy histograms of the counts of the heralded photons at D_{Ref} (a - dark) and D_{Trans} (b - dark) in 88010 seconds and with an energy conservation window of 1 keV. The spectrum of D_{Trig} (light) is shown for the comparison. The blue lines are calculated from theory and scaled vertically to match the total coincidence counts of D_{Ref}.

4.2. Nonclassical statistics of heralded photons

Next, I turn to confirm that the generated radiation is nonclassical. I first show that the correlation between the trigger photons and the photons measured by either D_{Trans} or D_{Ref}, within the experiment time window exhibits sub-Poissonian statistics. I calculate the degree of correlation $\sigma \equiv \dfrac{\left\langle \delta^2 \left(N_t - N_h \right) \right\rangle}{\left\langle N_t + N_h \right\rangle}$, where $\left\langle \delta^2 x \right\rangle = \left\langle x^2 \right\rangle - \left\langle x \right\rangle^2$ is the variance and the average $\left\langle \ \right\rangle$ is over the ensemble of detections by D_{Trig} and , N_t and N_h, are the number of the trigger photons detected by D_{Trig} and the heralded photons, measured at either D_{Trans} or D_{Ref}, respectively. The results plotted in Fig. 7 clearly show that σ approaching zero when applying either short time windows or narrow energy windows. This is a conclusive evidence that the generated radiation exhibits sub-Poissonian statistics, hence it is nonclassical. When the energy window is opened, σ increases with the time window, but it is always smaller than 1. This is because the rate of the accidental coincidences is increased but the probability to

14

measure two photons in the short time window is still low. σ decreases also when I narrow the time window but leave the energy conservation window open. When the energy conservation window is narrowed, σ is nearly zero for any time window that is used.

The functionality of the electronics that was described in chapter 3.3, explains also why the degree of correlation, σ that is presented in Fig. 7 is not identical to zero even when the stringent conditions for time windows and energy conservation were used. In order to show the gradual decrease of σ with the time window, I included detection events where the peak of one of the analog pulses was outside the maximal time window that was set for the software filter, as shown in Fig. 5, which is considered as a detection of only one photon (detector D_{Trig} in this example). These single detections can be within the energy conservation window if the energy of these photons is close to the energy of the pump photon. Such events contribute a non zero values to the average calculation at the numerator of σ .
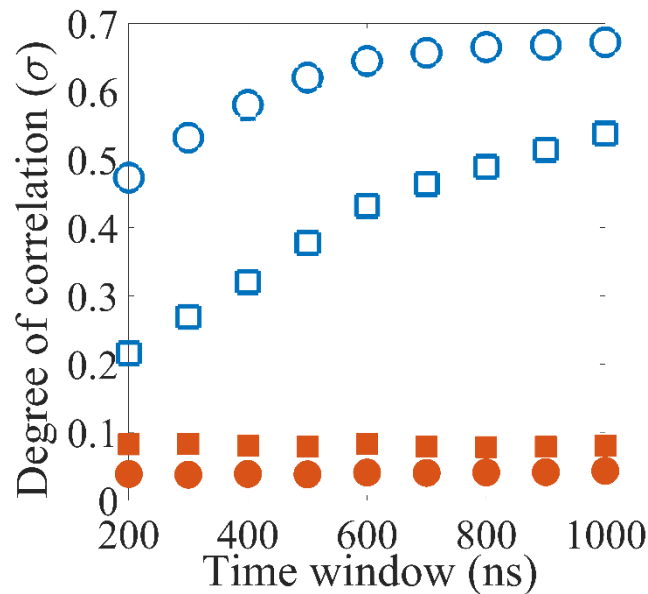
FIG. 7. The degree of correlation versus the coincidence time window for events satisfying the energy conservation within a tolerance of 1 keV (filled circles and rectangles) and for the total events (hollow circles and rectangles). The circles are for D_{Trans} and the squares are for D_{Ref}.

4.3. Single photon statistics

Now I turn to show that when the single photons interact with the beam splitter, they do not split in the sense I define in chapter 2.1. To verify this nonclassical nature

of the heralded photons and to ensure that despite the loss in the beam splitter, the quantum nature of the single photons is preserved, I measured the coincidences between the trigger detector and each of the output ports of the beam splitter. I applied the energy conservation to the sum of the photon energies of all three detectors since it is known that the sum of the photon energies of the trigger and heralded photons at the input of the beam splitter is equal to the photon energy of the pump photon. **As is clearly seen in Fig. 8(a), when the energy conservation window is narrow (1 keV), only heralded photons are observed, and no simultaneous clicks at both outputs of the beam splitter were measured. This is therefore the confirmation that the heralded x-ray photon cannot split.** For the comparison, I show measurements without imposing the photon energy window but for the same number of total counts in Fig. 8(b). Under this condition accidental coincidences were also measured, which are originated from stray radiation. Here we see simultaneous clicks at both outputs, which is an indication that more than one photon interacted with the beam splitter during one detection cycle. To verify that this observation is not fortuitous I show that the number of simultaneous clicks increases with the number of total counts in Fig. 8(c), which represents measurements with the same energy windows as in Fig. 8(b), but the total counts are higher by a factor of 100.
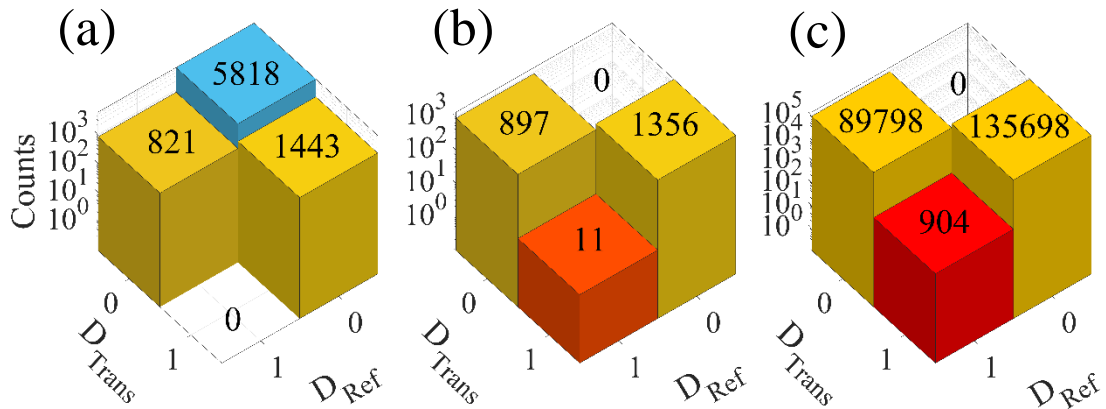
FIG. 8. Count histograms of the photons at the outputs of the beam splitter. In (a) I registered only heralded photons by using photon energy and time filters. In (b) and (c) I registered all the detected photons. In (a) and (b) the total number of events is 2264 and in (c) is 226400. The horizontal axes are the number of counts at each detector in one detection event. The zero-photon column is for events where only the trigger detector detects photons with photon energies in the selected range (since in (b) and (c) the energy window is wide open there are no counts in the zero-photon columns).

5. Discussion

To quantify the purity of the quantum state, I use the anticorrelation criterion [27,47,48],

$$\alpha = \frac{N_{Trig} N_{Trig-T-R}}{N_{Trig-T} N_{Trig-R}} \tag{3}$$

Here N_{Trig} is the total number of trigger events, in which D_{Trig} and at least one of the detectors D_{Trans} or D_{Ref} measure photons within a predefined energy window for each detector. N_{Trig-T} and N_{Trig-R} are the numbers of coincidences of D_{Trig} with D_{Trans} and D_{Ref}, respectively. $N_{Trig-T-R}$ is the number of triple coincidences between D_{Trans} and D_{Ref} and D_{Trig}. According to this criterion, for single photons, α is smaller than 1 while for classical beams is larger than 1.

For the heralded photons (Fig. 8(a)) α was found to be nominally zero, which is the indication of background-free quantum behavior. This is in contrast to most analog quantum optics experiments in the visible range in which α is smaller than 1 but finite [49,50]. Such high fidelity can be achieved thanks to the energy resolving capability and the negligible dark count rate of x-ray detectors. These superior characteristics, together with the nearly ideal efficiency are enabled by the high photon energy of the x-rays. This is a clear demonstration of the ability to perform background-free quantum optics experiments with x-rays.

Interestingly, α is smaller than 1 even when most of the detected photons are originated from stray radiation. The reason is that even with this radiation during a single measurement interval, only one photon interacts with the beam splitter on average and the probability that two photons interact with the beam splitter is much lower. This is because of the short coincidence time windows that were used to reduce the background in these experiments. Consequently, since a single photon is a single photon that cannot split regardless its origin, at most events there will be no simultaneous clicks at both output ports of the beam splitter leading to $\alpha < 1$. However, there is always a small probability that two simultaneous photons arrive, hence for the stray light α is not zero (for example α is 0.02 ± 0.006 and 0.0165 ± 0.0006 for Figs. 8(b) and 8(c), respectively. Further details are given in the table below). These results highlight that the anticorrelation criterion does not imply

that every measured photon was a single photon but only that on average single photons were measured.

In the following table I provide the measured counts that I used for the calculation of α:

Figure	N_{Trig}	N_{Trig-T}	N_{Trig-R}	$N_{Trig-T-R}$	α
Fig. 8(a)	8082	1443	821	0	0
Fig. 8(b)	2264	908	1367	11	0.02 ± 0.006
Fig. 8(c)	226400	90702	136602	904	0.0165 ± 0.0006

In summary, I showed in this work the direct evidence that x-ray photons are undividable quanta and it is a proof of principle experiment demonstrating efficient interaction of x-ray single photons with a beam splitter. Further improvements of the efficiency can be obtained by improving the match between the angular dispersion of the Bragg scattering of the beam splitter and the angular dispersion of the SPDC. This can be done by tuning the phase matching angles of the SPDC and by choosing a small Bragg angle and broad angular acceptance for the beam splitter. For interference experiments a more careful work is required in choosing the beam splitting crystal due to the random phases that a mosaic crystal might introduce. Nonetheless, this work shows an x-ray optical component that preserves quantum statistics and highlights the important parameters for an efficient beam splitter with x-ray single photon state. The single photon statistics that were observed, exhibit high fidelity despite the existence of loss and background noise in the setup. This work opens new possibilities for x-ray quantum optics by enabling experiments, which rely on beam splitters and single photon interactions. Further generalization of my work can lead to the development of novel sensitive and precise measurement techniques based upon x-ray single photon interferometry or NOON x-ray states.

6. Bibliography

[1]   E. Strizhevsky, D. Borodin, A. Schori, S. Francoual, R. Röhlsberger, and S. Shwartz, *Efficient Interaction of Heralded X-Ray Photons with a Beam Splitter*, Phys Rev Lett **127**, 13603 (2021).

[2]   E. Strizhevsky, D. Borodin, A. Schori, S. Francoual, R. Röhlsberger, and S. Shwartz, *Efficient Interaction of X-Ray Single Photons with a Beam Splitter*, in *Conference on Lasers and Electro-Optics*, edited by J. Kang Tomasulo, S., Ilev, I., Müller, D., Litchinitser, N., Polyakov, S., Podolskiy, V., Nunn, J., Dorrer, C., Fortier, T., Gan, Q., and Saraceno, C. (Optical Society of America, San Jose, California, 2021), p. FF2I.6.

[3]   R. Loudon, *The Quantum Theory of Light* (Oxford University Press, New York, 2000).

[4]   A. Authier, *Dynamical Theory of X-Ray Diffraction* (Oxford University Press, New York, 2001).

[5]   R. Röhlsberger, J. Evers, and S. Shwartz, *Quantum and Nonlinear Optics with Hard X-Rays*, in *Synchrotron Light Sources and Free-Electron Lasers: Accelerator Physics, Instrumentation and Science Applications*, edited by E. J. Jaeschke, S. Khan, J. R. Schneider, and J. B. Hastings (Springer International Publishing, Cham, 2020), pp. 1399–1431.

[6]   S. Send, A. Abboud, R. Hartmann, M. Huth, W. Leitenberger, N. Pashniak, J. Schmidt, L. Strüder, and U. Pietsch, *Characterization of a PnCCD for Applications with Synchrotron Radiation*, Nucl Instrum Methods Phys Res A **711**, 132 (2013).

[7]   J. W. Scuffham, M. D. Wilson, P. Seller, M. C. Veale, P. J. Sellin, S. D. M. Jacques, and R. J. Cernik, *A CdTe Detector for Hyperspectral SPECT Imaging*, Journal of Instrumentation **7**, P08027 (2012).

[8]   M. I. Kolobov, *Quantum Imaging* (Springer, New York, 2007).

[9]   G. Brida, M. Genovese, and I. Ruo Berchera, *Experimental Realization of Sub-Shot-Noise Quantum Imaging*, Nat Photonics **4**, 227 (2010).

[10]   P. A. Morris, R. S. Aspden, J. E. C. Bell, R. W. Boyd, and M. J. Padgett, *Imaging with a Small Number of Photons*, Nat Commun **6**, 5913 (2015).

[11]   S. Lloyd, *Enhanced Sensitivity of Photodetection via Quantum Illumination*, Science **321**, 1463 (2008).

[12]   M. J. Holland and K. Burnett, *Interferometric Detection of Optical Phase Shifts at the Heisenberg Limit*, Phys. Rev. Lett. **71**, 1355 (1993).

[13]   V. Giovannetti, S. Lloyd, and L. Maccone, *Quantum-Enhanced Measurements: Beating the Standard Quantum Limit*, Science **306**, 1330 (2004).

[14]   M. W. Mitchell, J. S. Lundeen, and A. M. Steinberg, *Super-Resolving Phase Measurements with a Multiphoton Entangled State*, Nature **429**, 161 (2004).

[15]   L. Pezzé, A. Smerzi, G. Khoury, J. F. Hodelin, and D. Bouwmeester, *Phase Detection at the Quantum Limit with Multiphoton Mach-Zehnder Interferometry*, Phys. Rev. Lett. **99**, 223602 (2007).

[16]   G. Y. Xiang, B. L. Higgins, D. W. Berry, H. M. Wiseman, and G. J. Pryde, *Entanglement-Enhanced Measurement of a Completely Unknown Optical Phase*, Nat Photonics **5**, 43 (2011).

[17]   V. Giovannetti, S. Lloyd, and L. Maccone, *Advances in Quantum Metrology*, Nat Photonics **5**, 222 (2011).

[18]   D. Attwood, *Soft X-Rays and Extreme Ultraviolet Radiation: Principles and Applications* (Cambridge University Press, Cambridge, 1999).

[19]   B. W. Adams, *Nonlinear Optics, Quantum Optics, and Ultrafast Phenomena with X-Rays: Physics with X-Ray Free-Electron Lasers* (Kluwer Academic Publisher, Norwell, MA, 2008).

[20]   M. O. Scully and M. S. Zubairy, *Quantum Optics* (Cambridge University Press, 1997).

[21]   Y. Yamamoto and A. Imamoglu, *Mesoscopic Quantum Optics* (John Wiley & Sons, New York, 1999).

[22]   D. F. Walls and G. J. Milburn, *Quantum Optics* (Springer-Verlag Berlin Heidelberg, Berlin, 1995).

[23]   D. Bouwmeester, A. K. Ekert, and A. Zeilinger, *The Physics of Quantum Information: Quantum Cryptography, Quantum Teleportation, Quantum Computation* (Springer, New York, 2000).

[24]   C. K. Hong, Z. Y. Ou, and L. Mandel, *Measurement of Subpicosecond Time Intervals between Two Photons by Interference*, Phys Rev Lett **59**, 2044 (1987).

[25]   A. C. Elitzur and L. Vaidman, *Quantum Mechanical Interaction-Free Measurements*, Found Phys **23**, 987 (1993).

[26]   A. G. White, J. R. Mitchell, O. Nairz, and P. G. Kwiat, ``*Interaction-Free'' Imaging*, Phys Rev A (Coll Park) **58**, 605 (1998).

[27]   P. Grangier, G. Roger, and A. Aspect, *Experimental Evidence for a Photon Anticorrelation Effect on a Beam Splitter: A New Light on Single-Photon Interferences*, Europhysics Letters (EPL) **1**, 173 (1986).

[28]   T. Jennewein, C. Simon, G. Weihs, H. Weinfurter, and A. Zeilinger, *Quantum Cryptography with Entangled Photons*, Phys Rev Lett **84**, 4729 (2000).

[29] P. Kok, H. Lee, and J. P. Dowling, *Creation of Large-Photon-Number Path Entanglement Conditioned on Photodetection*, Phys Rev A (Coll Park) **65**, 52104 (2002).

[30] S. Shwartz and S. E. Harris, *Polarization Entangled Photons at X-Ray Energies*, Phys. Rev. Lett. **106**, 80501 (2011).

[31] A. Pálffy, C. H. Keitel, and J. Evers, *Single-Photon Entanglement in the KeV Regime via Coherent Control of Nuclear Forward Scattering*, Phys. Rev. Lett. **103**, 17401 (2009).

[32] F. Vagizov, V. Antonov, Y. V Radeonychev, R. N. Shakhmuratov, and O. Kocharovskaya, *Coherent Control of the Waveforms of Recoilless γ-Ray Photons*, Nature **508**, 80 (2014).

[33] S. Shwartz, R. N. Coffee, J. M. Feldkamp, Y. Feng, J. B. Hastings, G. Y. Yin, and S. E. Harris, *X-Ray Parametric Down-Conversion in the Langevin Regime*, Phys. Rev. Lett. **109**, 13602 (2012).

[34] A. Schori, D. Borodin, K. Tamasaku, and S. Shwartz, *Ghost Imaging with Paired X-Ray Photons*, Phys. Rev. A **97**, 63804 (2018).

[35] S. Sofer, E. Strizhevsky, A. Schori, K. Tamasaku, and S. Shwartz, *Quantum Enhanced X-Ray Detection*, Phys Rev X **9**, 31033 (2019).

[36] A. K. Freund, A. Munkholm, and S. Brennan, *<title>X-Ray Diffraction Properties of Highly Oriented Pyrolytic Graphite</Title>*, in *Optics for High-Brightness Synchrotron Radiation Beamlines II*, edited by L. E. Berman and J. Arthur, Vol. 2856 (SPIE, 1996), pp. 68–79.

[37] S. M. Barnett, J. Jeffers, A. Gatti, and R. Loudon, *Quantum Optics of Lossy Beam Splitters*, Phys. Rev. A **57**, 2134 (1998).

[38] D. Borodin, A. Schori, F. Zontone, and S. Shwartz, *X-Ray Photon Pairs with Highly Suppressed Background*, Phys Rev A (Coll Park) **94**, 013843 (2016).

[39] J. F. Clauser, *Experimental Distinction between the Quantum and Classical Field-Theoretic Predictions for the Photoelectric Effect*, Physical Review D **9**, 853 (1974).

[40] L. Mandel, *Photoelectric Counting Measurements as a Test for the Existence of Photons*, J. Opt. Soc. Am. **67**, 1101 (1977).

[41] R. Loudon, *Non-Classical Effects in the Statistical Properties of Light*, Rep. Prog. Phys. **43**, 913 (1980).

[42] L. Mandel and E. Wolf, *Optical Coherence and Quantum Optics* (Cambridge University Press, Cambridge, 1995).

[43] R. H. BROWN and R. Q. TWISS, *Correlation between Photons in Two Coherent Beams of Light*, Nature **177**, 27 (1956).

[44] H. Legall, H. Stiel, V. Arkadiev, and A. A. Bjeoumikhov, *High Spectral Resolution X-Ray Optics with Highly Oriented Pyrolytic Graphite*, Opt Express **14**, 4570 (2006).

[45] I. Grigorieva, A. Antonov, and G. Gudi, *Graphite Optics—Current Opportunities, Properties and Limits*, Condens Matter **4**, (2019).

[46] J. Strempfer, S. Francoual, D. Reuther, D. K. Shukla, A. Skaugen, H. Schulte-Schrepping, T. Kracht, and H. Franz, *Resonant Scattering and Diffraction Beamline P09 at PETRA III*, J Synchrotron Radiat **20**, 541 (2013).

[47] A. B. U'Ren, C. Silberhorn, J. L. Ball, K. Banaszek, and I. A. Walmsley, *Characterization of the Nonclassical Nature of Conditionally Prepared Single Photons*, Phys. Rev. A **72**, 21802 (2005).

[48] M. Beck, *Comparing Measurements of G^(2)(0) Performed with Different Coincidence Detection Techniques*, Journal of the Optical Society of America B **24**, 2972 (2007).

[49] J. Zhao, C. Ma, M. Rüsing, and S. Mookherjea, *High Quality Entangled Photon Pair Generation in Periodically Poled Thin-Film Lithium Niobate Waveguides*, Phys. Rev. Lett. **124**, 163603 (2020).

[50] M. D. Eisaman, J. Fan, A. Migdall, and S. V Polyakov, *Invited Review Article: Single-Photon Sources and Detectors*, Review of Scientific Instruments **82**, 71101 (2011).

7. Appendix - Related Publications

Published works in peer review journals in which I took part during my research work:

- E. Strizhevsky, D. Borodin, A. Schori, S. Francoual, R. Röhlsberger, and S. Shwartz, *Efficient Interaction of Heralded X-Ray Photons with a Beam Splitter*, Phys. Rev. Lett. **127**, 13603 (2021).

- S. Sofer, E. Strizhevsky, A. Schori, K. Tamasaku, and S. Shwartz, *Quantum Enhanced X-Ray Detection*, Phys. Rev. X **9**, 31033 (2019).

- S. Sofer, O. Sefi, E. Strizhevsky, H. Aknin, S. P. Collins, G. Nisbet, B. Detlefs, C. J. Sahle, and S. Shwartz, *Observation of Strong Nonlinear Interactions in Parametric Down-Conversion of X-Rays into Ultraviolet Radiation*, Nat. Commun. **10**, 5673 (2019).

- O. Sefi, Y. Klein, E. Strizhevsky, I. P. Dolbnya, and S. Shwartz, *X-Ray Imaging of Fast Dynamics with Single-Pixel Detector*, Opt. Express **28**, 24568 (2020).

תקציר

עבודה זו היא ההדגמה הראשונה של מפצל אלומה (beam splitter) יעיל עבור פוטונים בודדים מוכרזים (heralded single photons) בקרינת X בעלי טווח אנרגיה של מספר קילו-אלקטרונוולטים. לאחר הוכחת יעילותו, השתמשתי במפצל אלומה זה כדי להראות את הסטטיסטיקה התת-פואסונית עבור מצב קרינה של פוטונים בודדים בקרינת X.

מפצלי אלומה הינם רכיבים יסודיים באופטיקה קוונטית המשמשים להדגמות של סופרפוזיציית מצבי פוטונים וקורלציות עוצמה, וכן נעשה בהם שימוש רב בתחומים שונים של אורכי גל. יחד עם זאת, אפילו עבור מקורות הפוטונים הבודדים היעילים ביותר בתחום קרינת ה- X, מפצלי האלומה הקיימים עדיין מאוד לא יעילים בגלל הרוחב האנרגטי והזוויתי של הפוטונים הנוצרים ממקורות אלו. בעבודתי זו אדגים שימוש בגביש מוזאי כמפצל אלומה יעיל. המונח גביש "מוזאי" (פסיפס) מתאר מודל של חוסר אידיאליות של הגביש. לפי מודל זה, גביש אמיתי מורכב מפסיפס של גבישים קטנים ביניהם יש חוסר אחידות ביישור הזוויתי. כדי להעריך את יעילות מפצל אלומה זה ולהשוות את תוצאות הניסוי עם התאוריה, ביתאתי בקירוב את עוצמת ההחזרה שלו באמצעות פונקציה אנליטית. על ידי הצבת פונקציה זו בחישוב נומרי הערכתי את הפרמטרים הדרושים לקבלת אינטרקציה יעילה בין פוטוני קרינת ה- X הבודדים לבין מפצל האלומה. הפוטונים הבודדים המוכרזים מתקבלים מזוגות פוטונים שנוצרים מאפקט ההמרה הפרמטרית הספונטנית של פוטון שואב בקרינת X הפוגע בגביש לא-ליניארי. החישוב הנומרי מנבא שהיחסים בין קצבי הפוטונים הבודדים המוכרזים המוחזרים והמועברים במפצל האלומה לבין הקצב שלהם לפניו הם $r_{R-Model} = 0.13$ ו- $r_{T-Model} = 0.17$ בהתאמה. מדדתי והשוותי את קצבי הפוטונים הבודדים המוכרזים עם ובלי מפצל האלומה ומצאתי שהקצבים ביציאות מפצל האלומה הם כ- 0.01 מניות לשניה שזה הוא ערך מאותו סדר הגודל של הקצב שנמדד ללא מפצל האלומה שהוא 0.0583±0.0099 מניות לשניה. הקצבים שמדדתי לאחר מפצל האלומה מראים שהוא יעיל מספיק למדידה וביצוע הדגמות של סטטיסטיקת פוטונים בודדים.

לאחר מדידת היעילות של מפצל האלומה, השתמשתי בו כדי להדגים את הסטטיסטיקה הקוונטית של הפוטונים המוכרזים. תחילה, וידאתי שמפצל האלומה משמר את הסטטיסטיקה התת-פואסונית על ידי בדיקה שמדידת הקורלציה של הפוטונים המוכרזים בשתי יציאות המפצל מתאפסת. לאחר מכן, ביצעתי את ההדגמה של אחד הניסויים היסודיים באופטיקה קוונטית – אינטרקציה של פוטון בודד עם מפצל אלומה. קיבלתי את התוצאה המפורסמת שפוטון בודד לא יכול להתפצל בין שתי יציאות המפצל – מדדתי 2264 פוטונים בודדים מוכרזים, כאשר כולם הוחזרו או עברו דרך המפצל אך לא נמדדו בו-זמנית בשתי היציאות.

הניסוי שלי מדגים את היתרון המשמעותי של קרינת X עבור אופטיקה קוונטית – היכולת לבצע מדידות בעלות דיוק גבוה ורעשי רקע זניחים. המדידות חסרות הרעש המעשי התאפשרו הודות לאנרגיה הגבוהה של פוטוני קרינת ה- X וגלאיי הסחיפה הסיליקוניים (silicon drift detectors). לגלאים אלו יש לא רק רעש רקע מאוד נמוך, אלא גם יכולת מדידה של מספרי הפוטונים הפוגעים והאנרגיות שלהם. החלק החסר בביצוע ניסויי אופטיקה קוונטית בקרינת X היה מפצל אלומה יעיל, והעבודה שלי מדגימה את השלמתו.

עבודה זו נעשתה בהדרכתו של

פרופ׳ שרון שוורץ

מהמחלקה לפיזיקה של אוניברסיטת

בר-אילן

אוניברסיטת בר-אילן

אינטרקציה יעילה בין פוטונים בודדים בקרינת X לבין מפצל אלומה

אדוארד סטריזׁיבסקי